Structural behaviour of arched steel beams with cellular openings

O.F. Zaher, N.M. Yossef *, M.H. El-Boghdadi, M.A. Dabaon

Department of Structural Engineering, Faculty of Engineering, Tanta University, Tanta, Egypt

A B S T R A C T

Arched beams with cellular openings (referred to here as arched cellular beams) are used as roof beams with several practical advantages and architectural-appearance requirements. This paper presents a discussion regarding the performance of arched cellular beams. An experimental program comprising four full-scale specimens was performed. The perforated cellular arched I-sections with hinged-hinged supports under a mid-span vertical concentrated load were tested. Manufacturing, material properties, boundary conditions, and the test setup are discussed in detail in this paper. The experimental investigation was carried out to study the effects of cellular web openings, subtended angles, and radii of curvature. The failure modes and key parameters were investigated. The web buckling resistance of the experimental specimens was calculated using two models from the literature. The analytical model for straight cellular beams proposed by Lawson et al. [1] yielded feasible conservative values for the critical buckling resistance of web posts for arched cellular beams. Finally, a finite element (FE) model is proposed to analyse the behaviour of arched cellular beams. It was validated by experimental results. The FE model accurately predicted the ultimate loads, the critical buckling loads and the failure modes of the tested specimens. It can be used for similar future studies.

© 2018 Elsevier Ltd. All rights reserved.

1. Introduction

A cellular beam is a modern type of a 'castellated beam' [2], and both are known as expanded beams. The solid sections of roof or floor beams could be replaced by expanded beams (castellated or cellular), where the web openings are used as passages for mechanical, electrical, and plumbing systems without increasing the height of ceilings, as well as reducing the cost of engineering services. Structurally, the vertical bending stiffness of the castellated beam is greater than the parent solid beam because of increasing the beam depth. In addition, cellular beams have sections with greater efficiency than castellated beams, where the cellular openings provide a more regular stress distribution as well as increased usable areas than any other opening shapes [3].

Castellated beams were first developed in the United States by the Chicago Bridge and Iron Works in 1910 [4], and since then, a wide range of web opening shapes have been studied [5–10]. Choosing the shape of the web opening depends upon the design purpose of the opening, and regular-shaped openings, for instance circular, are typically chosen. Using ANSYS software, a comparative analytical study for castellated and cellular beams was presented by Pachpor et al. [2]. The results showed that the von Mises stress is smaller in circular openings compared to hexagonal openings of the same area. The performance of cellular beams was investigated by Kuchta and Maslak [11]. Their study of cellular beam stability showed that the design procedures of cellular

beams should differ significantly from the solid parent beam. Therefore, the design equations of cellular steel beam were presented [1, 12–14]. Erdal and Saka [15] conducted experimental and finite element studies to establish the load-carrying capacity of non-composite cellular steel beams. Sheehan et al. [16] studied experimentally a long span composite cellular beam under flexural and shear stresses, and investigated the ability of composite beams to develop their plastic bending resistance with low degrees of shear connection.

A new type of web opening was proposed by forming a cellular beam with sinusoidal openings [17–20]. An analytical model, based on experimental tests and numerical simulations, was developed and discussed. The analytical model presented by Durif et al. [19] considered both the behaviour of each quarter around the openings and Vierendeel mechanisms. The analytical methods presented by Martin et al. [20] presented the criteria of the resistance of beams to Vierendeel bending and the resistance to the horizontal shear force in web-posts.

Currently, engineers incorporate arch-shaped beams into a variety of modern buildings and bridges. Because of their elegant shape, arches offer architects opportunities to express their ideas. Numerous studies have reported on the structural stability behaviour of solid steel arches, and design rules have been proposed for both in-plane buckling [21–23] and out-of-plane buckling [24–28].

Spoorenberg et al. [29, 30] studied the mechanical properties of roller-bent wide flange sections. The employment of a single bi-linear stress-strain relationship across the entire section led to a significant simplification of the analysis. The roll bending process has an impact on the material parameters. Based on the experimental and analytical

* Corresponding author.
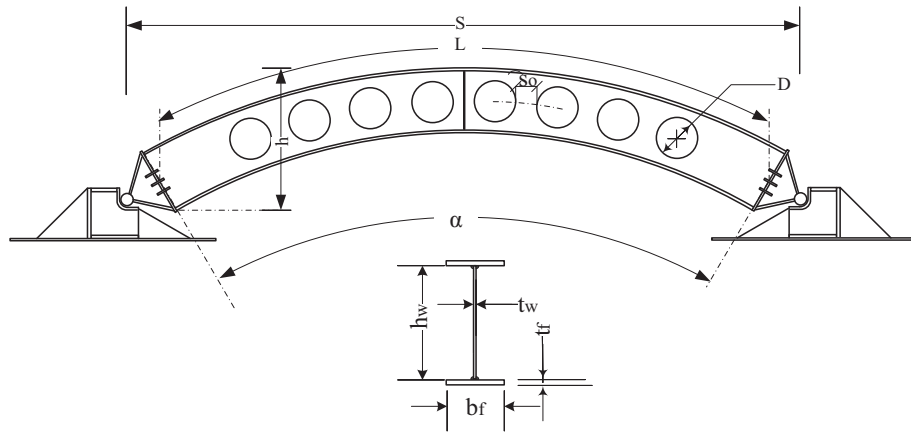*E-mail address:* nashwa_abdeltawab@f-eng.tanta.edu.eg (N.M. Yossef).

Fig. 1. Dimensions of test specimens.

results presented by Spoorenberg et al., a series of equations were proposed to obtain the stress-strain relationships for roller-bent wide flange steel arches.

However, previous studies on the structural behaviour of steel arch-shaped beams have focussed primarily on the arched beam with solid webs. Concerning the advantages of cellular beams, this paper presents an experimental investigation of an arch pin-ended steel I-section having cellular web openings under concentrated loads. The full-scale tests aim to: 1) Investigate the structural stability of steel arch-shaped beams with cellular web openings, 2) Focus on the buckling behaviour of the web, 3) Calibrate a finite element (FE) model with the load-deformation and load-strain relationships, 4) Discuss the experimental results and compare them with the analytical model presented in the literature, and 5) Propose and validate a detailed FE model with the experimental results. The FE model in this study is considered to be a preliminary analysis which was proposed and verified for similar future work.

2. Experimental program

In this section, the details of the experimental program are presented and discussed. This study is seen as an initial analysis to encourage similar future studies, using FE analysis.

2.1. Geometry of tested arches

To investigate the structural elastic-plastic stability of arched steel beams with cellular web openings, four manufactured arched steel specimens were tested: one with a solid web (B1), and three with cellular web openings (B2, B3, and B4). Two different spans and two subtended angles were chosen, such that the failure could be generated within the dimensions and the capacity of the test rig. The geometrical details of the test specimens are presented in Fig. 1 and Table 1, where h_w, t_w, b_f, and t_f are the web height, web thickness, flange width, and flange thickness respectively, L is the arc length, S is the span, α is the subtended angle in degrees, and h is the rise of the arch. For the cellular web openings, D is the hole diameter and s_o is the arched distance between the outer edges of the holes, which is taken as being equal to

0.5D, which gives $D/s_o = 2$ and $h_w = 1.5D$. The dimensions were chosen according to the BS EN 1993-1-1 [31] class 1 cross sections. These sections cover a significant range of beams primarily used as roof beams, and they can form a plastic analysis without any reduction of resistance due to local buckling. The depth of the circular web opening is small enough to prevent Vierendeel effects before web post buckling failure. Therefore, the hole diameter $D = 0.67\,h_w$ is chosen, such that web post buckling failure is expected. In order to focus on local failures of the cellular arched beams around the openings, lateral buckling of the beams was prevented by lateral supports.

It is noteworthy that in order to investigate the effect of web openings on obtaining a competitive advantage, the heights of solid specimen B1 and perforated test specimen B2 were 170 mm and 240 mm, respectively, such that they had the same weight. Therefore, test specimens B1 and B2 had the same weight, same developed arc length, and same angle of curvature.

2.2. Manufacturing

All webs and flanges of the arched specimens were cut from 4-mm- and 8-mm-thick flat plates, respectively. The webs, both solid or cellular, were cut in an arched shape, and then the flanges were welded to the arched web. Cellular specimens were perforated, with the holes cut in the solid beam achieved by cutting the required profiled holes out of a full-sized parent web. All parts of the beams (webs, flanges, holes, and stiffeners) were cut by a laser-cutting machine. The cutting procedure was managed by computer numerical control to ensure highly accurate dimensions. As opposed to cold bending, this type of assembly reduced the residual stresses in the cross sections.

In order to have full strain compatibility between the different components in the steel section, manual fillet welds were used to assemble different parts of the built-up cellular arched-beam specimens. The welding process was applied as follows:

1. Flange plates were spot welded to the web. The distance between two adjacent welding spots was 300 mm,
2. Tension plates were welded first, followed by the compression plates,

Table 1
Dimensions of test specimens.

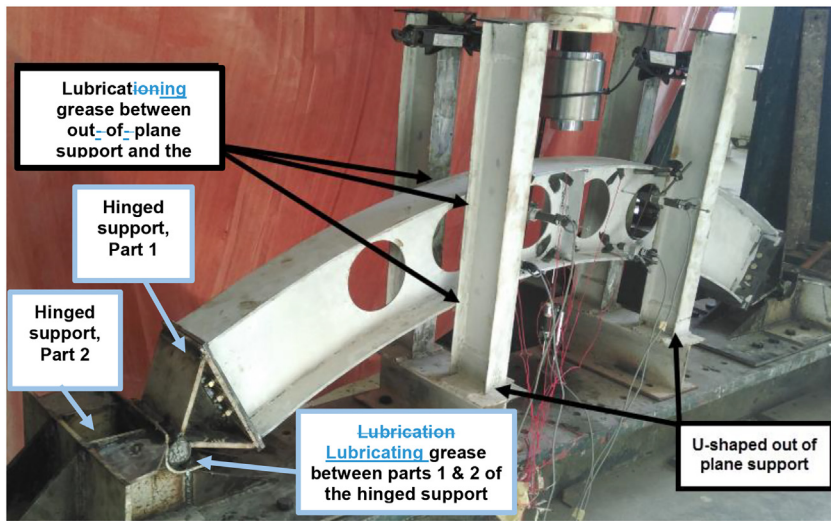| Specimen	Web height h_w [mm]	Web thickness t_w [mm]	Flange width b_f [mm]	Flange thickness t_f [mm]	Develop arc Length L [mm]	Span S [mm]	Arch rise h [mm]	Subtended angle α [degree]	Holes diameter D [mm]
B1	170	4	120	8	2451	2590	472	60	–
B2	240	4	120	8	2451	2590	538	60	160
B3	240	4	120	8	2651	2590	699	90	160
B4	240	4	120	8	2032	2190	484	60	160

Fig. 2. Test set up and supports.

3. For both tension and compression plates, the welding process was completed by welding from the ends to the middle, and

4. Continuous welds were divided into several partitions. The length of each partition was divided into 6 equal segments.

This welding procedure was used to reduce shrinkage strains and their associated stresses. By welding the tension flanges first, as well as welding from the ends to the middle, shrinkage movement was allowed within the beam curvature.

2.3. Boundary conditions and test setup

All tested arches were constrained by in-plane hinged supports as shown in Fig. 2. The hinged supports were connected to the ends of the perforated plate of the beam by six 12-mm-diameter high-strength bolts of grade 10.9, which were tightened by a torque wrench to 120 Nm. A 5-cm-diameter solid steel cylinder, covered with suitable lubrication grease, was used to ensure the in-plane rotation about its axis for a perfect hinged support.
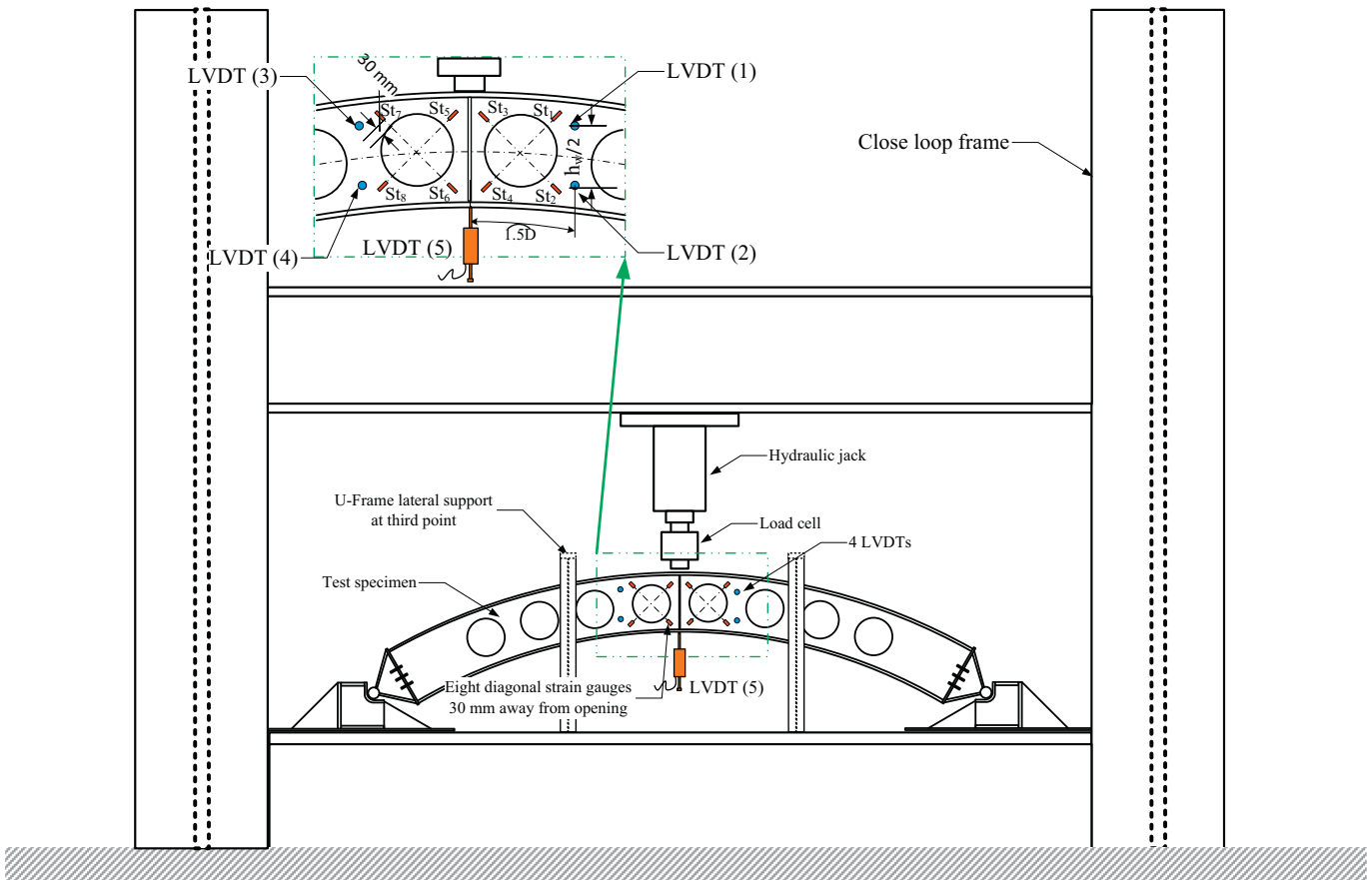

Fig. 3. Experimental setup and instrumentation.

Fig. 4. Complete test setup.

The hinged support was connected to the main test frame by 10 20-mm-diameter high-strength bolts of grade 8.8. These supports were designed to stop any horizontal movement at the ends of the specimen in any direction, except for rotation about the in-plane direction. Two vertical U-shaped supports were used to prevent the out-of-plane displacements at the third point of the span. A lubricating grease was used at the contact points to ensure that the specimens could move span-wise and vertically, as shown in Fig. 2.

A vertical load was applied at the mid span on the top flange of the arch using a hydraulic jack of 1000 kN capacity, as shown in Figs. 3 and 4. The load on the beam was gradually applied in increments of approximately 5 kN steps, and it was monotonically increased until the end of the test after a number of unloading-reloading cycles at the beginning of the elastic domain.

2.4. Material properties

In order to determine the material properties of the steel plates used in the test specimens, three tensile coupons were cut from the 4-mm-and 8-mm-thick web and flange plates, respectively. The coupon dimensions conformed to the Australian Standard AS1391 [32] for the tensile testing of metals, based on a gauge length of 100 mm, and the average yield stress (f_y), the modulus of elasticity (E_s), and the ultimate stress (f_u) are presented in Table 2.

2.5. Instrumentation

For the cellular beams, tensile and compressive forces were applied close to the top and the bottom of the web post because of the horizontal shear. Therefore, the stresses varied around the openings. To evaluate the strains around the openings, the area around the mid-span openings was divided into four equal segments, and a strain gauge was bonded 30-mm radially from the cell edge for each segment, to avoid excessive distortion at the edge of the openings. Eight strain gauges were used for each specimen. The mid-span openings were chosen, assuming that the failure would occur around the web opening at the maximum moment. The lateral displacement of the web and the vertical displacement of the tested specimens were measured using linear variable differential transformers (LVDTs). The out-of-plane displacements of the web-posts of the cellular and solid web were measured by four and two LVDTs, respectively. In addition, one LVDT was used to measure the deflection under the applied load. The

arrangement of the LVDTs and strain gauges are shown in Figs. 3 and 4. The loads, displacements, and strains were recorded automatically by the data acquisition system.

3. Experimental results

This study was conducted to determine the effect of web openings together with the effects of changing the span and subtended angle on the behaviour of arched cellular beams. The results and the primary parameters specifying the behaviour of the cellular arched specimens and their failure modes are presented in Table 3, where $P_{u,Exp}$ is the ultimate load carrying capacity, which is the maximum load observed in the test, and was typically followed by a drop in the load value, $P_{cr,Exp}$ is the vertical load at which the web-post began to buckle, which was followed by an increase in the web lateral displacements observed from the LVDT readings, and $\delta_{u,Exp}$ is the maximum vertical displacement measured at the ultimate load under the loaded point.

All specimens were tested up to failure, and the various parameters are discussed in the following sections.

3.1. General observations and modes of failure

A detailed analysis of the test result shows that the web openings of the perforated specimens weakened the arched beams as expected. The cellular arched specimens B2, B3, and B4 were affected by the stability of the web posts, and they failed because of web post buckling, as shown in Fig. 5. The web post buckling initiated when the applied load attained the critical load $P_{cr,Exp}$. When the applied loads approached its ultimate value, the web post buckling failures were clearly visible. On the other hand, the solid arched beam B1 developed a plastic hinge and failed because of flexural strength, as shown in Fig. 6.

Specimens B1 and B2 had the same subtended angle and span, but different web depths. Specimen B2 was perforated to have the same weight as the solid specimen B1. Results from the tests indicate that the ultimate load of specimen B1 was approximately double the ultimate load of specimen B2, and the percentage increase of the ultimate deflection for specimen B1 compared with specimen B2 was approximately 86%, as shown in Fig. 7.

3.2. Effect of subtended angles

Specimens B2 and B3 had the same web depths, flanges, and spans, but different subtended angles. The curves shown in Fig. 8 are for load-deflection and out-of-plane load displacements for specimens B2 and B3. The curves indicate that the behaviours of specimens B2 and B3 are similar; however, B3 has a greater ultimate load than B2. The lateral displacement of both specimens was negligible until reaching the critical load $P_{cr,Exp}$, where buckling of the web was observed, and the yield of the web was noticeable.

Table 2
Steel properties of test specimens.

Plate thickness (mm)	Yield stress f_y (N/mm^2)	Modulus of elasticity (E_s) (MPa)	Ultimate stress f_u (N/mm^2)
4	242	205×10^3	290
8	233	199×10^3	315

Table 3
Experimental results.

Tested specimens	Ultimate load $P_{u, Exp}$ (kN)	Critical load $P_{cr, Exp}$ (kN)	Ultimate deflection $\delta_{u, Exp}$ (mm)	Failure mode
B1	253	204	44	Flexural
B2	124	121	24	Web post buckling
B3	137	133	18	Web post buckling
B4	130	129	17	Web post buckling
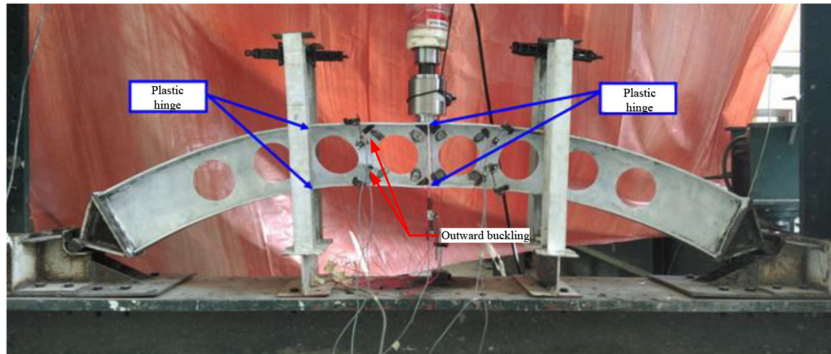
Fig. 5. Web post buckling of cellular arched beam B2.

Fig. 9 shows the load-strain curves around the web opening on the left side of the load (see Fig. 3). The strains around the opening were small up to the critical load, except for the strains closer to the loading point (St5) where greater strains were observed early on because of the concentrated load.

Although it was interesting to note that (St7) and (St8) indicated positive strains, this was plausible if we consider the compressive and tensile stresses acting in the web post suggested by Lawson et al. [1], as shown in Fig. 10. The compressive and tensile stresses depend on the equilibrium of normal stress ϭ and shear stresses τ around the web post as shown in Fig. 11. The authors are of the opinion that the horizontal reaction of the arched beam results in an internal axial force, which increases the normal compressive stress of the upper tees ($\unicode{x03ED}_u$), and reduces the normal tension stress of lower tees ($\unicode{x03ED}_L$). The equilibrium of the normal and shear stresses of the arched web post cause an increase and reduction in the compressive and tension stresses in the web post, respectively, and can explain the outward buckling observed experimentally and the tension of both strains (St7) and (St8), as shown in Fig. 5. However, the presence of the vertical stiffener was the primary reason for this phenomenon not having the same influence on the (St5) and (St6) readings.

Figs. 8 and 9 show the effects of the subtended angle on the critical load. When the web begins to buckle it also affects the beam strength, such that the beam strength increases with increasing subtended angle. This is a consequence of the arch action effect, as high internal axial forces are generated in the beam. As the subtended angle increases, this effect increases and increased arching action takes place.

However, in spite of the span differences between B3 and B4, the effect of the arch action because of the increase of subtended angles was observed in the ultimate load, as shown in Table 3. The impact of the arched action on the horizontal shear is not identical to the effect of the equilibrium of the normal stress at the web opening caused by the internal axial force. A more detailed analysis of the impact of the radius of curvature and the internal axial force on the horizontal shear will be discussed in the next section.

3.3. Effect of reducing radius of curvature

Beams B2 and B4 have the same cross sections and subtended angles, but differing spans and, therefore, different radii of curvatures. Fig. 12 shows the load-displacement curves for specimens B2 and B4, where it can be seen that specimen B4, with the shorter span and smaller radius of curvature ($R_{B4} = 1940$ mm), has a negligible advantage at maximum strength and higher stiffness than specimen B2 ($R_{B2} = 2340$ mm). The increase in the maximum strength could be attributed to the smaller radius of curvature, as decreasing the radius of curvature decreases the internal axial force (for the same
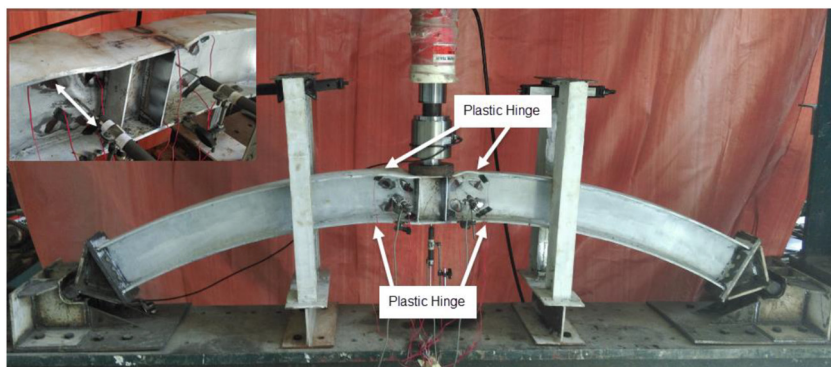

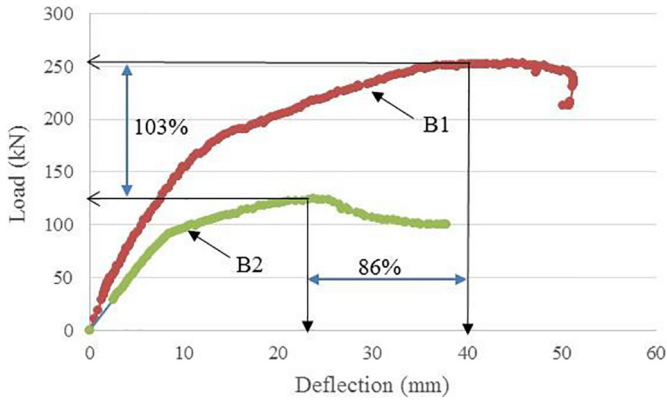Fig. 6. Flexural failure mode of solid arched beam B1.

Fig. 7. Effect of web opening on load-deflection curves of tested specimens B1 and B2.

Fig. 10. Web post buckling model in cellular beam presented by Lawson et al. [1].

subtended angle). This has a greater impact on the value of the horizontal shear, as Lawson et al. [1] reported that the horizontal shear depends on the equilibrium of the shear and normal stresses. An alternate explanation is that on decreasing the horizontal shear, as a result of reducing the internal axial force, the compressive stress decreases which initiates local buckling.

The two specimens have the same behaviours, as can be clearly seen in Fig. 12, the lateral displacements of the web were negligible up to the
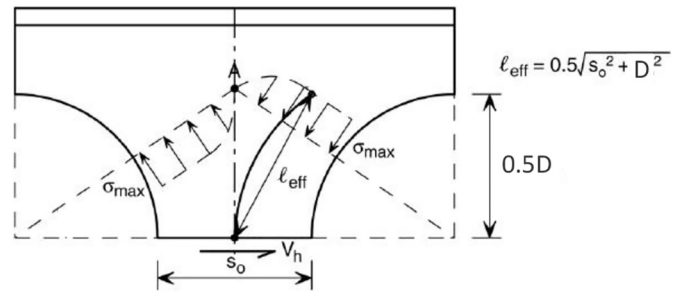
critical buckling load, and then the web lateral displacement increased to failure.

4. Analytical model

Failure of castellated beams have been reported in a number of studies [7, 11, 13, 33]. Six primary failure modes have been described: 1) lateral torsional buckling, 2) shear failure, 3) bending failure, 4) Vierendeel yielding, 5) web post welding fracture, and 6) web post buckling. The latter three modes are classified as local failure modes of beams with web openings. Previous studies [1, 33–35] revealed that the failure
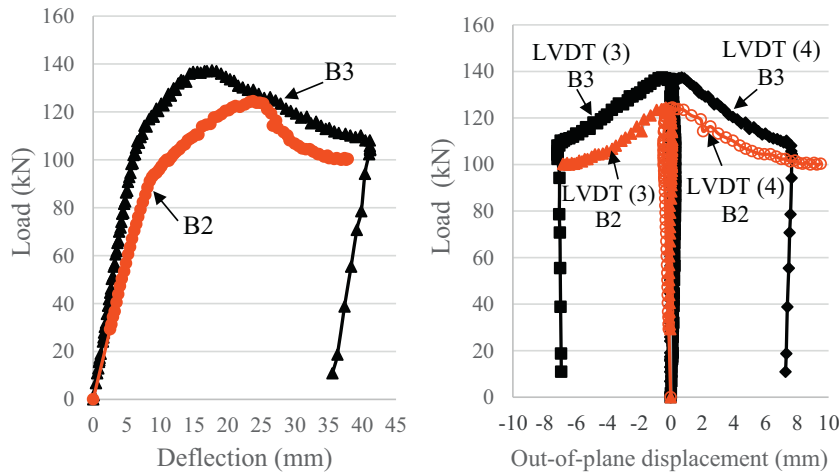

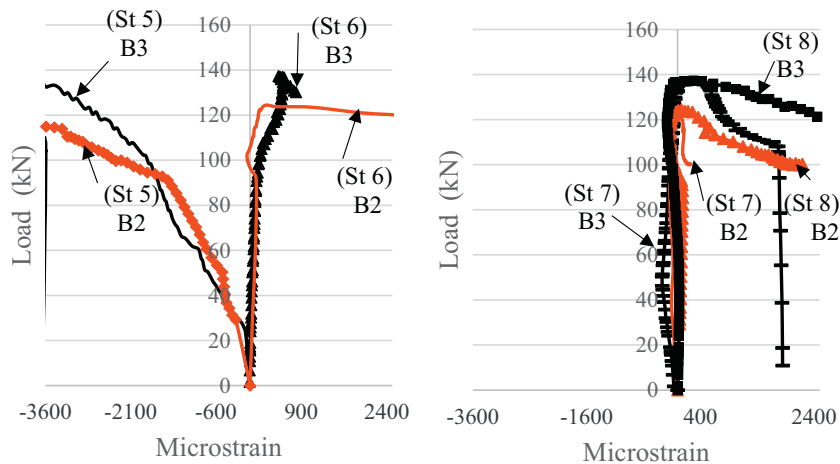Fig. 8. Load-displacement curves for specimen B2 and B3.

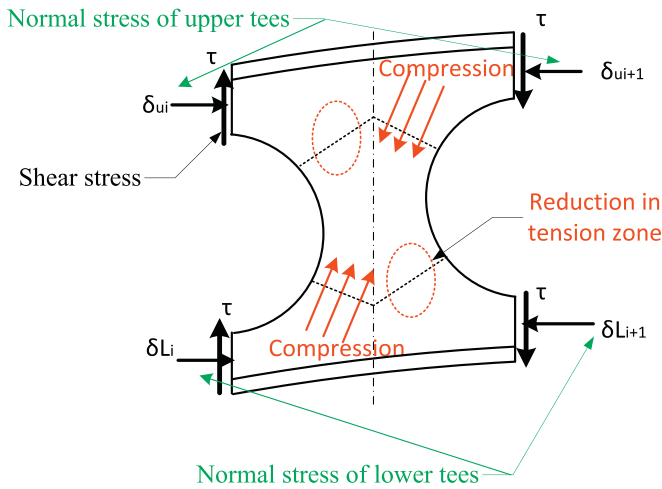Fig. 9. Load-strain curves for specimens B2 and B3.

Fig. 11. Web post buckling model for tested arched beam.

modes of cellular and castellated beams are similar [1, 33, 34], and, therefore, the analytical models for castellated beams were adapted to cellular beams [35].

As web post buckling was the failure mode of the cellular specimens as presented in the previous section, the analytical design approaches of web post buckling for straight cellular beams will be discussed for arched beams. The primary objective of the analytical model was to validate the suitability of the simplified literature models of straight cellular beams to calculate the buckling load of arched cellular beams based on experimental study.

The analytical model adapted by Panedpojaman et al. [13] and Lawson et al. [1] for cellular straight beams are used here to calculate the web post buckling load $P_{cr,Rd}$ for arched cellular beams. The strut model presented by Lawson is based on the effective length of the compression field [1] and modelled as a strut in the web post. The effective

buckling length of the compression strut, shown in Fig. 10, calculated by Lawson was as follows:

$$l_{e,Lawson} = 0.5 \sqrt{s_o^2 + D^2} \qquad (1)$$

The compressive force (P_c) in the strut was then calculated according to BS EN 1993-1-1 [31]. The calculated compressive force is used to compute the horizontal shear strength V_h, as follows:

$$V_h = P_c b_e t_w \qquad (2)$$

where b_e is the effective width of the web post taken as $s_o/2$. Note that the horizontal shear strength presented by Eq. (2) was assumed to be equal to half of the shear resistance at the web opening ($V_{cr,Lawson}$). The strut model presented by Lawson was simple, and it calculated the shear resistance by taking the effect of the distance between holes (s_o) and the diameter of the holes (D), as presented in Table 4.

Panedpojaman et al. suggested that the tee height (d) also resisted the buckling and should be taken into account [13]. Therefore, the effective buckling length of the compression strut calculated by Panedpojaman was as follows:

$$l_{e,Panedpojaman} = k * 0.5 \sqrt{s_o^2 + D^2} \qquad (3)$$

where k is the coefficient of the effective buckling length calculated as follows:

$$k = 0.9 \left(\frac{D + s_o}{D}\right) \left(\frac{D}{d}\right)^2 \qquad (4)$$

The comparison between the two models and the experimental results is presented in Table 4.

The experimental web buckling resistance force was calculated as the internal shear at the web opening of the plane with an angle (α')
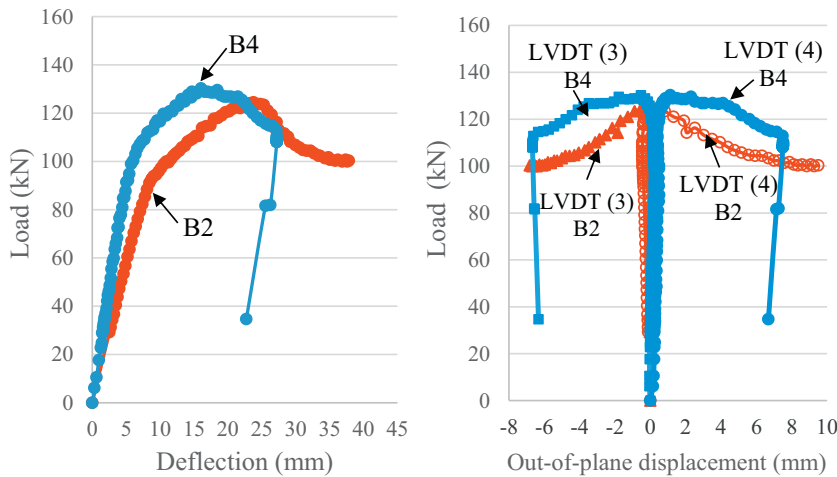

Fig. 12. Load-displacement curves for specimens B2 and B4.

Table 4
Comparison between experimental and analytical shear force at web opening.

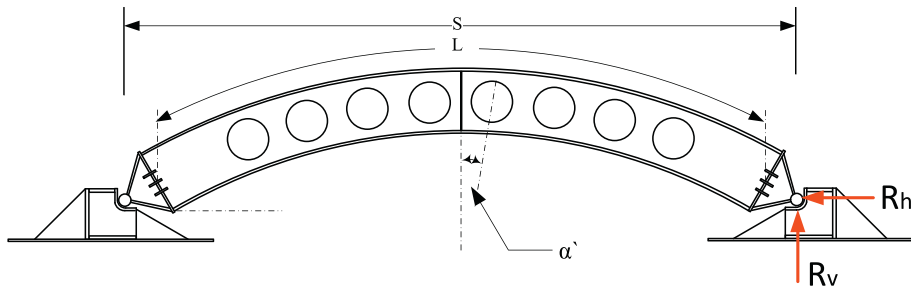| Specimen	Experimental buckling load $P_{cr,Exp}$ (kN)	Experimental web buckling resistance $V_{cr, Exp}$ (kN)	Web buckling resistance by Lawson $V_{cr, Lawson}$ (kN)	$\frac{V_{cr,Lawson}}{V_{cr,Exp}}$	Web buckling resistance by Panedpojaman $V_{cr, Panedpojaman}$ (kN)	$\frac{V_{cr,Panedpojaman}}{V_{cr,Exp}}$
B2	121	53	49	0.93	66	1.26
B3	133	59		0.83		1.13
B4	129	55		0.89		1.21
		Mean		0.88		1.2

Fig. 13. Internal shear at critical section for arched experimental beam.
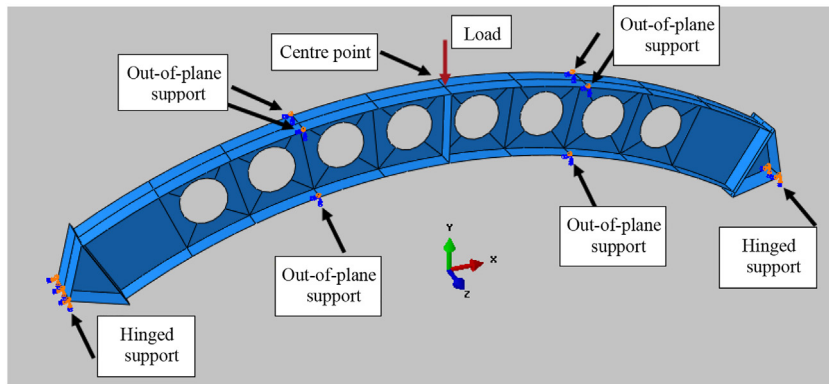
Table 5
Boundary condition in specimens.

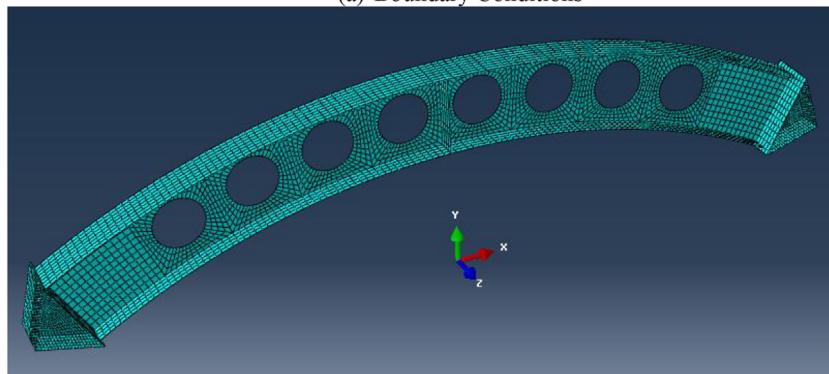| Support	U_x	U_y	U_z	θ_x	θ_y	θ_z
Hinged support	1	1	1	1	1	0
Out-of-plane support	0	0	1	1	1	0

1 = restrained 0 = free.

measured from the vertical axis as shown in Fig. 13, and is calculated as follows:

$$V_{cr,Exp} = R_{v,Exp}\ \cos(\alpha') - R_{h,Exp}\ \sin(\alpha') \qquad (5)$$

where $R_{v,Exp}$ and $R_{h,Exp}$ are the vertical and horizontal reactions at the experimental buckling load, respectively.

(a) Boundary Conditions

(b) FE Mesh

Fig. 14. Boundary conditions and FE mesh used to simulate test specimens.

Table 6
Comparison between experimental and FE results.

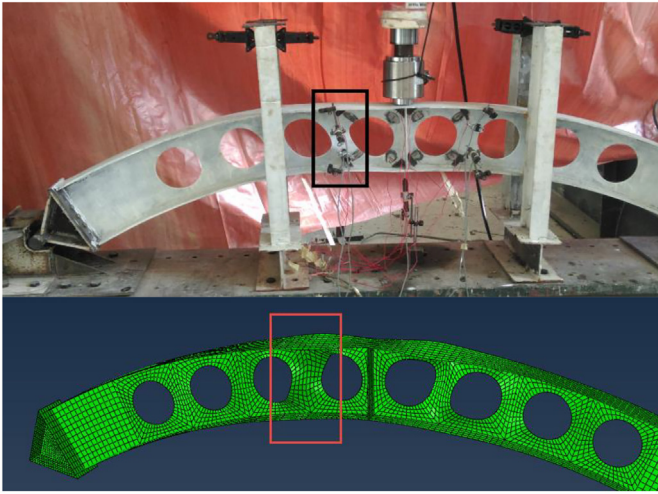| Specimen	Exp. Ultimate Load $P_{u,\ Exp}$ (kN)	FE. Ultimate Load $P_{u,\ FE}$ (kN)	$\frac{P_{u,Exp}}{P_{u,FE}}$	Exp. Buckling Load $P_{cr,\ Exp}$ (kN)	FE. Buckling Load $P_{cr,\ FE}$ (kN)	$\frac{P_{cr,Exp}}{P_{cr,FE}}$	Exp. Ultimate Deflection $\delta_{u,Exp}$ (mm)	FE. Ultimate Deflection $\delta_{u,FE}$ (mm)	$\frac{\delta_{u,Exp}}{\delta_{u,FE}}$
B1	253	229	1.10	204	199	1.03	44	31	1.41
B2	124	128	0.97	121	122	0.99	24	17	1.36
B3	137	132	1.04	133	124	1.07	18	12	1.45
B4	130	127	1.02	129	119	1.08	17	16	1.02
Mean			1.03			1.04			1.31
Standard deviation			0.05			0.04			0.19

Fig. 15. Comparison between experimental and FE failure mode of arched cellular beam B2.

The comparison shows that the Lawson model was more conservative than Panedpojaman model, and that the modification made by Panedpojaman may not be suitable for arched cellular beams, as normal forces appear because of the curvature effects on the value of the shear resistance at the web openings.

Although the Lawson model presents a simplified conservative method to calculate buckling resistance of cellular arched webs, future studies should target an accurate analytical model for arched cellular beams, taking into account the effect of the subtended angle, based on a large-scale parametric study. The FE model discussed in the following section will provide a powerful tool for this large-scale parametric study.

5. Finite element model

A detailed FE model was developed and verified by the experimental results. Nonlinear simulations of the arched steel beams with cellular openings were introduced. The proposed FE model will be used by the authors to promote similar future studies.

5.1. Model description

The ABAQUS software [36] was used in developing the FE model. The S4R shell element, having four nodes each with six degrees of freedom, was used to model the tested specimens (flanges, web, and part-1 of the hinged support). The 3D model allows the significant deformations and local instability effects to be monitored, and both material and geometric nonlinearities were considered. The bilinear elastic-plastic stress-strain curve with linear strain hardening was used to simulate the steel. The modulus of elasticity and yield strength were obtained from tensile coupon tests, and, for the hardening part of the curve, a modulus of 2 GPa was used. To simulate the hinged supports, the edge line nodes at the supports were prevented from moving in any direction, except for rotation in the plane of curvature, as presented in Table 5.

The FE mesh was chosen by a guide run. The mesh that provided adequate accuracy and minimum computational time in modelling the
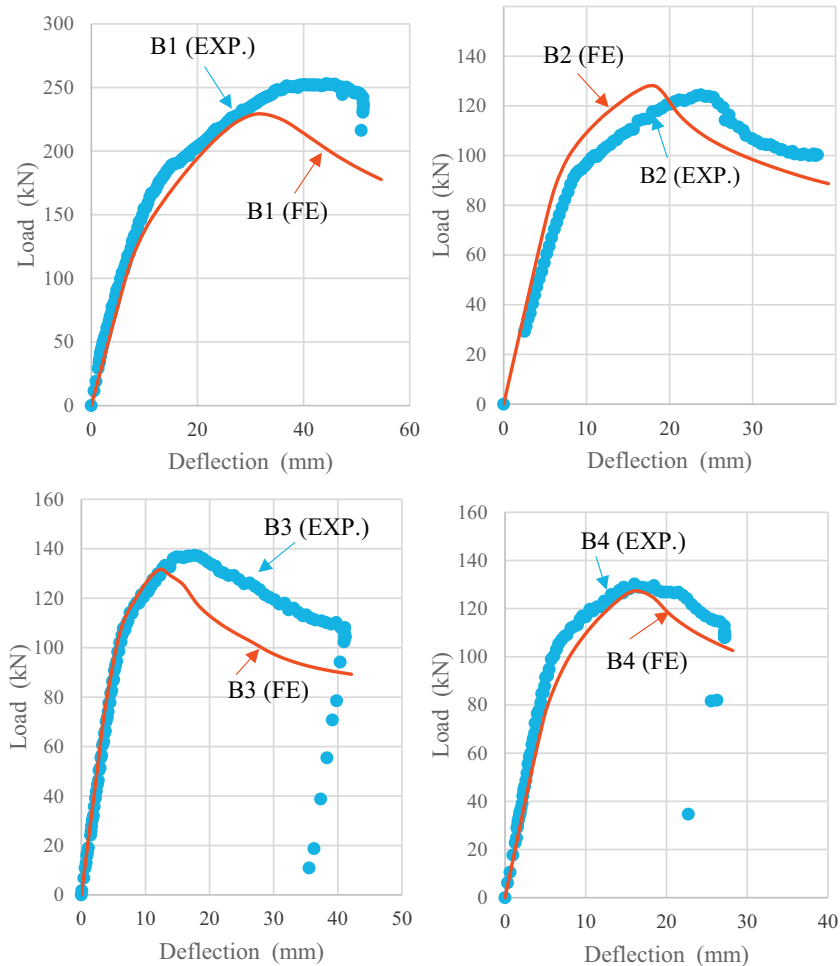

Fig. 16. Comparison between experimental and FE load-deflection curves.
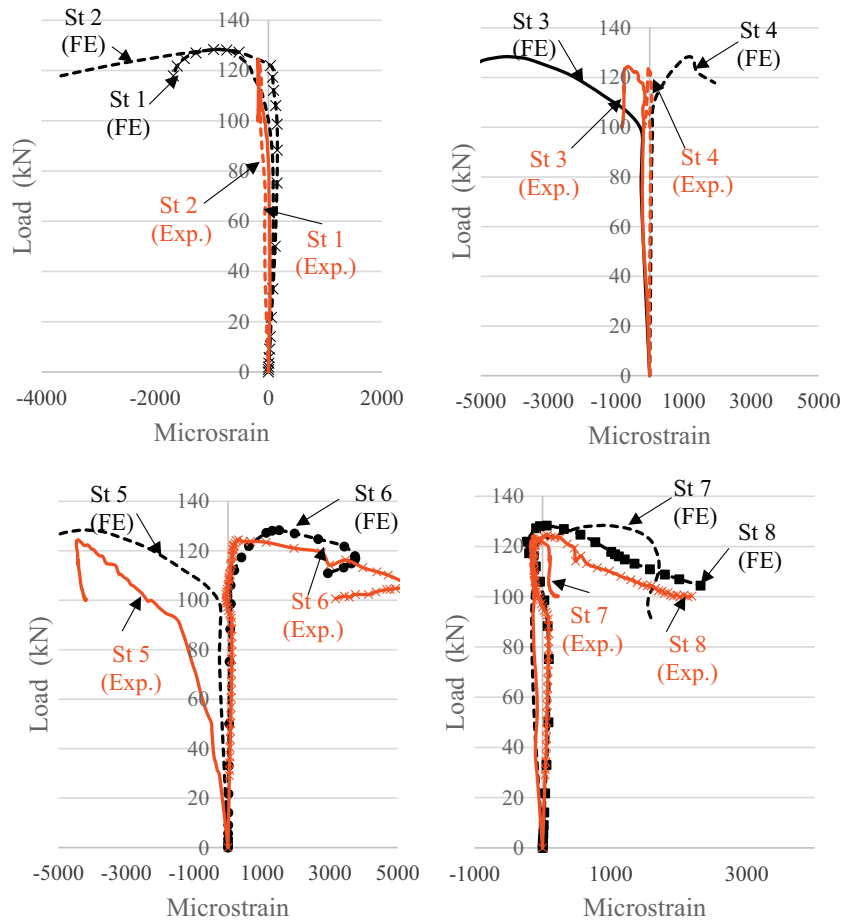
Fig. 17. Comparison between experimental and FE load-strain curves for specimen B2.

specimens was chosen such that the aspect ratio of the elements did not exceed 1:3. The boundary conditions and the FE mesh used are shown in Fig. 14.

Initial local geometric imperfections, as a result of fabrication and transportation processes, are typically found in beams. Therefore, superposition of local buckling modes with measured magnitudes was recommended for accurate FE analysis. Bowing of the web was incorporated during modelling to simulate geometric imperfections of the tested specimens. The bowing shape was introduced by a buckling mode in the Eigenvalue linear buckling analysis available in the ABAQUS library [36]. The measured values were introduced with scale factors between $(h_w/200)$ to $(h_w/250)$, which considers a greater value for the bow of the web.

5.2. Model validation

The FE model was validated to determine its accuracy. The model was used to simulate the behaviour of arched cellular beam. Table 6 presents the comparison between the FE results and the experimental tests.

The mean values of $\frac{P_{u,Exp}}{P_{u,FE}}$, $\frac{P_{cr,Exp}}{P_{cr,FE}}$, and $\frac{\delta_{u,Exp}}{\delta_{u,FE}}$ are 1.03, 1.04, and 1.31, with standard deviations of 0.05, 0.04, and 0.19, respectively. The failure modes of the FE model were compared with the failure of the tested specimens in Fig. 15, which indicates a good agreement with the experimental results. Fig. 16 presents a comparison between the experimental and the FE load-deflection curves for the four specimens, where it can be seen that the FE model accurately predicts the load-deflection curves for the tested specimens in terms of initial stiffness, strength, and maximum deflection. Figs. 17 and

18 show a comparison between the experimental and the FE load-strain curves of the B2 and B3 specimens, respectively. It can be seen that the FE model accurately predicts the load strain curves for the tested specimens. In general, the FE model simulates the behaviour of cellular arched beam with good agreement.

It is important to note that the experimental ultimate mid-span deflection values are greater than those of the numerical analysis, and the mean value of $\frac{\delta_{u,Ex}}{\delta_{u,FE}}$ is 1.31 with a standard deviation of 0.19. The difference between the experimental and numerical ultimate deflections could be a result of the simplification of the numerical model, such as the simplified stress-strain curve taken as bilinear, and the non-consideration of residual stresses.

6. Conclusions

In this study, the behaviour of arched cellular beams under static concentrated loads were investigated experimentally. Four test specimens were perforated and loaded to failure. The deflection and web lateral displacements were monitored, and the strains around the holes were recorded. The failure modes and the experimental measurements were presented and discussed. The effects of changing the subtended angles and the beam radii of curvature were discussed. Two literature models, for calculating the web post buckling load of straight cellular beams, were assessed to calculate the buckling load of tested beams. The FE model was developed based on the experimental geometry and compared with the test results. The following conclusions were drawn based on this experimental investigation. However, caution must be taken in applying these conclusions to long-span cellular beams.
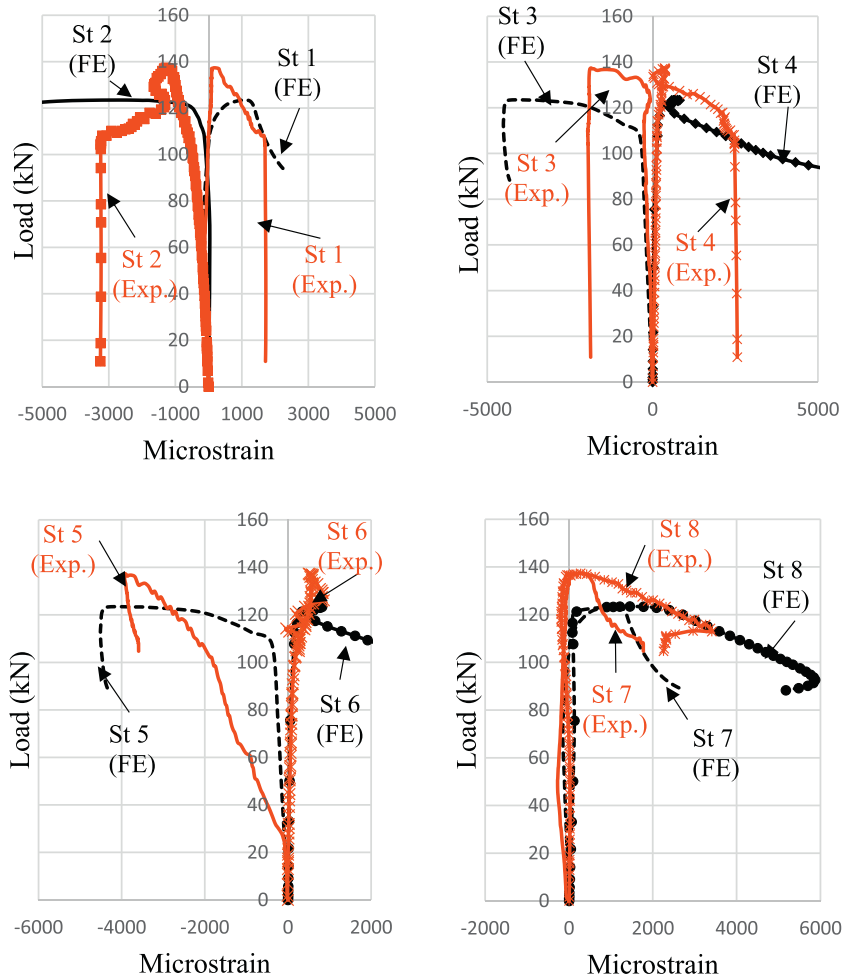
Fig. 18. Comparison between experimental and FE load-strain curves for specimen B3.

1. Despite the advantage of cellular beams, the results from the experimental study indicated that a significant decrease in the ultimate strength of cellular beams was observed compared to the solid beams $\frac{(P_{u,exp} \ of \ B1}{P_{u,exp} \ of \ B2 \cdot 100\%=203\%)}$.

2. The experimental tests of the cellular beams indicated that, by increasing the subtended angle, the ultimate strength increased, as did the buckling load for the web posts. In addition, reducing the beam length, in other words decreasing the radius of curvature, is inversely proportional to the ultimate strength of the arched cellular beam.

3. The analytical model for straight cellular beams reported by Lawson et al. [1] provided a reasonable conservative value for the critical buckling resistance of web posts for curved cellular beams, as the web buckling resistance calculated by Lawson yielded an average of 0.88 $(\frac{V_{cr,Lawson}}{V_{cr,Exp}}=0.88)$ of the web buckling resistance determined experimentally for the arched web. The modification presented by Panedpojaman et al. [13] for calculating the web post buckling resistance was not applicable to arched webs $(\frac{V_{cr,Panedpojaman}}{V_{cr,Exp}}=1.2)$.

4. The proposed FE model used to simulate cellular curved beams, which showed good accuracy, was compared with the experimental results. The experimental and FE model results, including load-deflection curves, load-strain curves, ultimate load, buckling load, and ultimate deflection, were in good agreement, as were the failure modes.

This study raised numerous questions that require further study, using the proposed FE model, to determine whether filling both openings close to the load could prevent the failure in the first web-posts and could result in a more representative stress field in the failure sections. In the future, additional numerical analyses for long-span arched cellular beams with distributed loads could provide further insight.

References

[1] R.M. Lawson, J. Lim, S.J. Hicks, W.I. Simms, Design of composite asymmetric cellular beams and beams with large web openings, J. Constr. Steel Res. 62 (6) (2006) 614–629.
[2] P.D. Pachpor, N.D. Mittal, L.N. Gupta, N.V. Deshpande, Finite element analysis and comparison of castellated and cellular beam, Adv. Mater. Res. 264–265 (2011) 694–699.
[3] N.D. Lagaros, L.D. Psarras, M. Papadrakakis, G. Panagiotou, Optimum design of steel structures with web openings, Eng. Struct. 30 (2008) 2528–2537.
[4] L. Amayreh, M.P. Saka, Failure load prediction of castelleted beams using artificial neural networks, Asian J. Civil Eng. 6 (2005) 35–54.
[5] J.P. Boyer, Castellated Beams - New Developments, The AISC National Engineering Conf, Omaha, Nebr, 1964.
[6] M.A. Dabaon, M.I. El-Naggar, N.M. Yossef, Experimental and theoretical study of curved rolled and castellated composite beams Alex, Engl. J. 42 (2003) 219–230.
[7] P. Wang, Q. Ma, X. Wang, Investigation on Vierendeel mechanism failure of castellated steel beams with fillet corner web openings, Eng. Struct. 74 (2014) 44–51.
[8] K.F. Chung, C.H. Liu, A.C.H. Ko, Steel beams with large web openings of various shapes and sizes: an empirical design method using a generalised moment-shear interaction curve, J. Constr. Steel Res. 59 (9) (2003) 1177–1200.
[9] T.C.H. Liu, K.F. Chung, Steel beams with large web openings of various shapes and sizes: finite element investigation, J. Constr. Steel Res. 59 (9) (2003) 1159–1176.
[10] P. Wang, K. Guo, M. Liu, L. Zhang, Shear buckling strengths of web-posts in a castellated steel beam with hexagonal web openings, J. Constr. Steel Res. 121 (2016) 173–184.
[11] K. Kuchta, M. Maslak, Failure modes determining the resistance and the stability of steel cellular beams, J. Civil Eng. Environ. Archit. 62 (2015) 263–280.

[12] P. Panedpojaman, T. Rongram, Design Equations for Vierendeel Bending of Steel Beams With Circular Web Openings, The World Congress on Engineering 2014, London, U.K., 2014

[13] P. Panedpojaman, T. Thepchatri, S. Limkatanyu, Novel design equations for shear strength of local web-post buckling in cellular beams, Thin-Walled Struct. 76 (2014) 92–104.

[14] P. Panedpojaman, T. Thepchatri, S. Limkatanyu, Novel simplified equations for Vierendeel design of beams with (elongated) circular openings, J. Constr. Steel Res. 112 (2015) 10–21.

[15] F. Erdal, M.P. Saka, Ultimate load carrying capacity of optimally designed steel cellular beams, J. Constr. Steel Res. 80 (2013) 355–368.

[16] T. Sheehan, X.D.D. Lam, E. Aggelopoulos, M. Lawson, R. Obiala, Experimental study on long spanning composite cellular beam under flexure and shear, J. Constr. Steel Res. 116 (2016) 40–54.

[17] S. Durif, A. Bouchaïr, O. Vassart, Experimental tests and numerical modeling of cellular beams with sinusoidal openings, J. Constr. Steel Res. 82 (2013) 72–87.

[18] S. Durif, A. Bouchaïr, O. Vassart, Experimental and numerical investigation on web-post specimen from cellular beams with sinusoidal openings, Eng. Struct. 59 (2014) 587–598.

[19] S. Durif, A. Bouchair, Analytical model to predict the resistance of cellular beams with sinusoidal openings, J. Constr. Steel Res. 121 (2016) 80–96.

[20] P.-O. Martin, M. Couchaux, O. Vassart, A. Bureau, An analytical method for the resistance of cellular beams with sinusoidal openings, Eng. Struct. 143 (2017) 113–126.

[21] Y.-L. Pi, N.S. Trahair, In-plane buckling and design of steel arches, J. Struct. Eng. 125 (11) (1999) 1291–1298.

[22] Y.-L. Pi, M.A. Bradford, In-plane strength and design of fixed steel I-section arches, Eng. Struct. 26 (3) (2004) 291–301.

[23] Y.-L. Guo, H. Chen, Y.-L. Pi, M.A. Bradford, In-plane strength of steel arches with a sinusoidal corrugated web under a full-span uniform vertical load: experimental and numerical investigations, Eng. Struct. 110 (2016) 105–115.

[24] C. Dou, Y.-L. Guo, S.-Y. Zhao, Y.-L. Pi, Experimental investigation into flexural-torsional ultimate resistance of steel circular arches, J. Struct. Eng. ASCE 141 (10) (2015).

[25] Y.-L. Guo, S.-Y. Zhao, Y.-L. Pi, M.A. Bradford, C. Dou, An experimental study on out-of-plane inelastic buckling strength of fixed steel arches, Eng. Struct. 98 (2015) 118–127.

[26] Y.-L. Pi, N.S. Trahair, Out-of-plane inelastic buckling and strength of steel arches, J. Struct. Eng. 124 (2) (1998) 174–183.

[27] D.B.L. Poutré, R.C. Spoorenberg, H.H. Snijder, J.C.D. Hoenderkamp, Out-of-plane stability of roller bent steel arches — an experimental investigation, J. Constr. Steel Res. 81 (2013) 20–34.

[28] Y.-L. Pi, M.A. Bradford, Out-of-plane strength design of fixed steel I-section arches, J. Struct. Eng. 131 (4) (2005) 560–568.

[29] R.C. Spoorenberg, H.H. Snijder, J.C.D. Hoenderkamp, Mechanical properties of roller bent wide flange sections — part 1: experimental investigation, J. Constr. Steel Res. 68 (1) (2012) 51–62.

[30] R.C. Spoorenberg, H.H. Snijder, J.C.D. Hoenderkamp, Mechanical properties of roller bent wide flange sections — part 2: prediction model, J. Constr. Steel Res. 68 (1) (2012) 63–77.

[31] EC3, Eurocode 3, Design of steel structures-, Part 1-1: General rules and rules for buildings, British Standards Institution, BS EN 1993-1-1, London, UK, 2005.

[32] Australian Standard, Methods for Tensile Testing of Metals. AS 1391, Standards Association of Australia, Sydney, Australia, 1991.

[33] K.F. Chung, T.C.H. Liu, A.C.H. Ko, Investigation on Vierendeel mechanism in steel beams with circular web openings, J. Constr. Steel Res. 57 (5) (2001) 467–490.

[34] F. Erdal, E. Doğan, M.P. Saka, Optimum design of cellular beams using harmony search and particle swarm optimizers, J. Constr. Steel Res. 67 (2) (2011) 237–247.

[35] S. Durif, A. Bouchaïr, O. Vassart, Validation of an analytical model for curved and tapered cellular beams at normal and fire conditions, Period. Polytech. 57 (2013) 83–95.

[36] ABAQUS Standard User's Manual, The Abaqus Software Is a Product of Dassault Systèmes Simulia Corp, DassaultSystèmes, Providence, RI, USA, 2008.